Simulated electromagnetic emissions in the ionosphere: On possible signatures of non-linear wave interaction in digital data

Daniel Söderström

IRF Scientific Report 282
June 2003

ISSN 0284-1703

INSTITUTET FÖR RYMDFYSIK

Swedish Institute of Space Physics

Uppsala, Sweden

Stimulated Electromagnetic Emissions in the Ionosphere: On Possible Signatures of Non-linear Wave Interaction in Digital Data

Daniel Söderström

19th June 2003

Abstract

När en högfrekvent elektromagnetisk våg skickas upp i jonosfären kan den excitera många olika typer av processer i radiovågens reflektionsområde. Vissa av plasmaprocesserna sänder i sin tur ut elektromagnetisk strålning, vilken kan tas emot av antenner på jorden. Information om dessa processer kan fås genom att analysera det mottagna spektrat. I detta arbete analyseras spektrat genom att olika delar av det korskorreleras. Genom att jämföra korkorrelationen för vitt brus med korskorrelationen i det mottagna spektrat visas att strålningen så som den detekteras på marken har samma karaktär som vitt brus, även om strålningens frekvensspektrum är systematiskt strukturerat. Det visas även, att standardavvikelsen är konstant när antalet värden i medelvärdesbildningen ökas. Detta är vad som även observeras då signalen består av vitt brus.

When a high frequency electromagnetic wave is transmitted into the ionosphere, many types of processes can be excited in the wave reflection region. Some of these plasma processes in turn emit electromagnetic waves, which can be received by antennas on the ground. By analysing the received spectrum, information about the processes can be obtained. By comparing the cross-correlation for white noise with the cross-correlation for different parts of the spectrum, it is shown in this work that the radiation detected on the ground has the same character as white noise, although the frequency spectrum of the detected radiation is systematically stuctured. It is also shown that when averaging the cross-correlation values, the standard deviation stays more or less constant when increasing the number of values in the mean. This is also the case when the signal consists of white noise.

Contents

List of Figures

Chapter 1

Introduction

Almost everywhere we look, we see time series. It could be the variation of sunspots, ocean waves or electric signals from the brain. A part of the time series analysis is the spectral analysis which is used frequently and extensively in many areas of the physical sciences.

The time series in this work comes from measurements of Stimulated Electromagnetic Emissions, or SEE for short. SEE is the radiation you get from Earth's ionosphere when you perturb the plasma located there with a powerful high frequency electromagnetic wave. This radiation was discovered in 1981 while performing experiments with high frequency waves at the Heating facility near Tromsø in Norway. The high frequency waves transmitted from the ground excited many types of processes in the ionospheric plasma that in turn emitted electromagnetic radiation. It now became possible to study non-linear processes excited by high frequency pumping without the need of probing electromagnetic waves, such as used in radars.

Just a time series does not show much information, but a Fourier transform of the series and a plot of the corresponding power spectrum, provides a clearer picture. Now the different spectral features can be seen and conclusions about their origins can be drawn. There is, however, more information buried in the time series than the power spectrum shows. More refined methods must therefore be employed.

The year 1948 marked the beginning of modern spectral analysis when John W. Tukey and Maurice Barlett independently took a crucial step. Tukey took the cosine transform of the auto-covariance and found the power spectrum [3]. Since then there has been great development in the area of spectral analysis, not the least thanks to the enormous increase in computational power. Large amounts of data can now be handled and analysed in a multitude of ways.

In this work, the data from two experimental campaigns has been analysed with a method called cross-correlation. It is a statistical method that can correlate different parts of, for example, a spectrum. Or, in other words,

check if there is some connection between two spectral features.

Today, still very little is known about the SEE. Certain theories exists, which try to explain how these processes are excited. But some theories contradict each other. It is the aim of this work to begin to look at the signals from the experiments, initiate further investigations and perhaps shed some light on the different types of processes; to confirm or contradict the theories available.

Chapter 2

Earth's Ionosphere

As most people probably know, Earth has an atmosphere consisting of different gases, mostly hydrogen, nitrogen and oxygen. If it had not been for the sun and cosmic rays, the atmosphere would have remained neutral, that is not ionised, and there would be no ionosphere.

2.1 Creation of the Ionosphere

Earth is constantly bombarded with high energy photons from the sun and high energy particles from our galaxy. If the photons have the right energy, they may ionise the neutral atoms in Earth's atmosphere. Typically, solar photons in the "extreme" ultraviolet and the ultraviolet wavelength range produce the dayside ionosphere. The high energy particles may also ionise (precipitate) the neutral atoms if they have more energy than the binding energy of the atoms. A high energy particle may ionise more than one atom if it has enough energy, since it looses energy gradually at each ionisation as it moves through the atmosphere. A photon is, however, absorbed in a single event. The ionisation process produces free electrons and ions in a mix, called a plasma, which constitute Earth's ionosphere [4].

Because of the gradient in the atmospheric density (the density is higher on the ground than at an altitude of, say, 300 km) and the fact that the photon flux and particle energy flux decreases with decreasing altitude, the ion density will produce peaks at certain altitudes depending on the mechanism of ionisation. Of course the free electrons and ions can recombine to form neutral atoms again, so a state of equilibrium is reached where recombination is balanced by ionisation.

2.2 Determining Ionospheric Density

Since the ionosphere consists of charged particles, it would be expected to interact with an electric field, such as that in an electromagnetic wave.

Indeed, that is what is seen when an electromagnetic wave is transmitted into the ionosphere.

The plasma can, if disturbed, oscillate with a certain frequency determined by the electron density. High density means that the electrons are close to each other and disturbances can propagate with higher speed than if the electrons were separated by a greater distance. If an electromagnetic wave with frequency lower than the ionospheric plasma frequency is transmitted into the ionosphere, it will "bounce" back to Earth. This can be utilised when transmitting a radio message around the world. If the frequency of the electromagnetic wave is higher than the plasma frequency, the wave can propagate into space. Thus, the ionosphere sets a lower limit to the frequency we can use in our communication with space.

Transmitting an electromagnetic wave of known frequency vertically into the ionosphere and noting the delay time if it bounces and returns, it can be calculated at what height it bounced and the plasma density at that height. This is done with an ionosonde.

2.3 Plasma Density Profile

By sweeping the frequency the ionosonde gives a picture of how the plasma density in the bottom side ionosphere varies with altitude. At the dayside of Earth, this plasma density profile shows three prominent peaks called the D, E and F region. The D region is located below 90 km which means that only the most energetic ionisation sources can reach this region. The E region located between 90 and 130 km is mostly produced by ultraviolet radiation (100–150 nm) and solar x-rays (1–10 nm), and therefore almost disappears on the night side of Earth. The F region is the most prominent peak in the plasma density profile and it is located above 130 km [4].

Increasing the power of the electromagnetic wave transmitted into the ionosphere, it can cause turbulence in the plasma. In the turbulence electrons are accelerated whereby they emit electromagnetic radiation. By studying these phenomena, new insight in plasma processes can be gained. This takes us to the next section which deals with these experiments.

Chapter 3

Stimulated Electromagnetic Emissions

When a powerful high frequency electromagnetic wave, a pump wave, is transmitted into the ionosphere from the ground, it can excite many types of processes in the plasma. Some of these processes emit electromagnetic radiation, called stimulated electromagnetic emissions (SEE), with frequencies around the pump wave frequency f_0. This radiation can be studied with a variety of techniques, for example by just monitoring the electromagnetic radiation on the ground. The pump frequency used is of high frequency (HF), that is a few MHz, near the plasma frequency in the area of interaction, usually at an altitude of 200–300 km. The spectral width of the SEE is of the order of 100 kHz [1]. Depending on the frequency and duty cycle of the pump wave, different spectral features can be observed in the SEE spectrum. This is schematically illustrated in figure 3.1.

For long pump duration, that is high pump duty cycle, the downshifted maximum (DM) is a prominent feature. It is observed to be downshifted about 8-12 kHz ($\Delta f_- = \Delta f_{DM} \approx 8 - 12$ kHz) from the pump frequency. When approaching the critical frequency of the ionospheric plasma from above, the DM is the first spectral feature to be excited. The DM feature can not be seen when the pump wave is close to a multiple of the electron gyro frequency f_e [1].

The DM can also be followed by a cascade of nDM ($n = 2, 3, 4$) emissions, each successively weaker and at successively lower frequencies [1]. The 2DM is typically downshifted with 1-2 kHz less than $2\Delta f_{DM}$. Experiments indicate that the 2DM is excited through the lower half of the DM spectrum in a cascade type process [1].

Associated with the DM is a upshifted maximum (UM) located upshifted from the pump wave at about the mirror frequency of the DM, and 10-20 dB weaker in amplitude than the DM [1].

Another SEE spectral feature is the broad upshifted maximum (BUM).

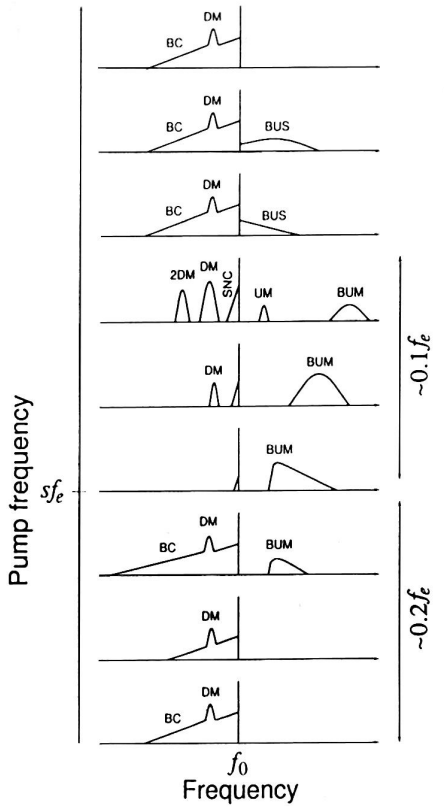

FIGURE 3.1: *Schematic diagram of SEE spectra for long thermal time scales for different pump wave frequencies f_0 relative to sf_e ($s > 3$), where f_e is the electron gyro frequency. The spectrum changes as we pass the electron gyro frequency from below. Taken from [1].*

This feature exists above the pump frequency at $\Delta f_+ \approx 15 - 200$ kHz and is excited for f_0 close to and slightly above multiples of the electron gyro frequency sf_e. It has been observed for $s = 3 - 7$ [1].

In the present work the cross-correlation between 2DM and DM, DM and BUM, DM and UM, within the BUM and within another spectral feature called the broad continuum (BC), appearing below the DM, will be studied. Data considered comes from two experiments performed at the Sura facility near Vasilsursk, Russia, in 1998 and at the EISCAT–Heating facility near Tromsø, Norway, in 1999. The data files are labelled sura98_n and trom99_n, respectively, where _n denotes the file number.

Chapter 4

The Quadrature Detector

The SEE are received by an antenna on the ground connected to an analogue-to-digital converter. No intermediate electronics, such as amplifiers, filters or detectors, are employed; the signal is sampled digitally directly from the antenna [5]. The output sample rate from the analogue to digital converter was in the Sura 98 and Tromsø 99 campaign set to 320 kHz. A digital version of the quadrature detector discussed below was then applied on the digital signal to get the in-phase and quadrature-phase channels. For simplicity only the analogue quadrature detector will be discussed below, to give an idea of how it works.

To get some information, for example the phase, from the SEE detected by an antenna a detector of some sort is used. The quadrature detector schematically illustrated in figure 4.1 takes the signal, $A(t)$, received from the antenna and passes it through a band-pass filter to extract the frequency components of interest. The signal is then normally (but not in the case of the SEE data) amplified and fed through a power splitter, which splits the signal into two parts. Each signal is then fed through a mixer which multiplies its two incoming signals. One signal is the output from the power splitter and the other from a local oscillator. If the local oscillator signal is

$$L(t) = E_L \cos(\omega_L t + \phi_L)$$

and the incoming antenna signal is assumed to be

$$A(t) = E_0 \cos(\omega_0 t + \phi_0) + E_- \cos(\omega_- t + \phi_-) + E_+ \cos(\omega_+ t + \phi_+)$$

the output signal from the detector is

$$\begin{aligned} O(t) = A(t)L(t) = {} & E_0 \cos(\omega_0 t + \phi_0) E_L \cos(\omega_L t + \phi_L) \\ & + E_- \cos(\omega_- t + \phi_-) E_L \cos(\omega_L t + \phi_L) \\ & + E_+ \cos(\omega_+ t + \phi_+) E_L \cos(\omega_L t + \phi_L). \end{aligned} \quad (4.1)$$

where ω_0 is a central frequency component and ω_- and ω_+ are downshifted and upshifted frequency components, respectively and ϕ_0, ϕ_-, ϕ_+ are arbitrary phases. This can be rewritten with some help from trigonometric relations as

$$O(t) = \frac{1}{2}E_0E_L\{\cos[(\omega_0 - \omega_L)t + (\phi_0 - \phi_L)] + \cos[(\omega_0 + \omega_L)t + (\phi_0 + \phi_L)]\}$$
$$+ \frac{1}{2}E_-E_L\{\cos[(\omega_- - \omega_L)t + (\phi_- - \phi_L)] + \cos[(\omega_- + \omega_L)t + (\phi_- + \phi_L)]\}$$
$$+ \frac{1}{2}E_+E_L\{\cos[(\omega_+ - \omega_L)t + (\phi_+ - \phi_L)] + \cos[(\omega_+ + \omega_L)t + (\phi_+ + \phi_L)]\} \tag{4.2}$$

If the frequency of the local oscillator, ω_L, is chosen to be close or of the

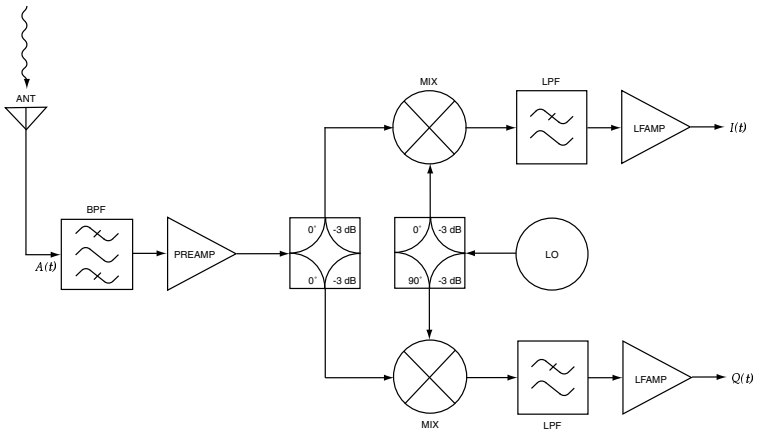

FIGURE 4.1: *Schematic diagram of the quadrature detector. The antenna signal $A(t)$ is processed to give a quadrature- ($Q(t)$) and a in-phase ($I(t)$) signal. After [2].*

same order as the frequency ω_0, we see that the difference terms in equation (4) will be of low frequency, while the sum terms will be of high frequency. Filtering the output signal $O(t)$ through a low-pass filter will remove the high frequency terms and the result will be

$$I(t) = \frac{1}{2}E_0E_L\cos[(\omega_0 - \omega_L)t + (\phi_0 - \phi_L)]$$
$$+ \frac{1}{2}E_-E_L\cos[(\omega_- - \omega_L)t + (\phi_- - \phi_L)]$$
$$+ \frac{1}{2}E_+E_L\cos[(\omega_+ - \omega_L)t + (\phi_+ - \phi_L)]. \tag{4.3}$$

If $\omega_L = \omega_0$ it can be seen that the signal (4.3) will consist of one constant term and two oscillating terms. Thus, frequencies equal to ω_L will be shifted

to zero frequency. This is advantageous, since the sampling frequency need not be so high to cover the frequencies of interest, if the antenna signal is, for example, in the megahertz frequency range.

The second signal from the power splitter is multiplied by the same local oscillator, except that a 90° phase delay is added to the local oscillator. This is equal to multiplying by a sine wave and we get after filtering the signal through a low-pass filter

$$\begin{aligned} Q(t) = \frac{1}{2}E_0E_L\sin[(\omega_0-\omega_L)t+(\phi_0-\phi_L)] \\ + \frac{1}{2}E_-E_L\sin[(\omega_--\omega_L)t+(\phi_--\phi_L)] \\ + \frac{1}{2}E_+E_L\sin[(\omega_+-\omega_L)t+(\phi_+-\phi_L)]. \end{aligned} \quad (4.4)$$

The output in (4.3) is called the in-phase channel and the output in (4.4) is called the quadrature-phase channel. These two channels can be considered to be a complex-valued signal $S(t) = I(t) + \mathrm{i}Q(t)$, called the analytic signal.

Chapter 5

Digital Signal Processing

Just the plain time series from the antenna does not give much information. It must be analysed by some means. One way to get more information from the time series is to do a Fourier transform of the same and plot the power spectrum $P(\omega) = \sum_{t=-\infty}^{\infty} X(t)X^*(t)e^{-i\omega t}$, where $X(t)$ is the time series and the asterisk denotes the complex conjugate. This gives information about the distribution of the signal over frequency. There is, however, more information buried in the time series that disappears when the power spectrum is calculated. To extract that information, higher order spectral analysis methods can be used. The next sections deals with the cumulants, which are the fundamental building blocks for spectral analysis, and their spectra.

5.1 Cumulants and Cumulant Spectrum

Having a stationary time series $\mathbf{X}(t),\ t = 0, \pm 1, \ldots$ with the vector components $X_a(t),\ a = 1, \ldots, r$ and $E|X_a(t)|^k < \infty$, we define [6]

$$c_{a_1,\ldots,a_k}(t_1, \ldots, t_k) = \mathrm{cum}(X_{a_1}(t_1), \ldots, X_{a_k}(t_k))$$

for $a_1, \ldots, a_k = 1, \ldots, r$ and $t_1, \ldots, t_k = 0, \pm 1, \ldots$. The quantity $c_{a_1,\ldots,a_k}(t_1, \ldots, t_k)$ is called the joint cumulant of order k of the series $\mathbf{X}(t)$.

The rth order joint cumulant $\mathrm{cum}(Y_1, \ldots, Y_r)$ of $(Y_1, \ldots, Y_r)$ is defined by the coefficient of $\frac{(i\xi)^n}{n!},\ n = 1 \ldots r$ in the Taylor series expansion of $K(\xi) = \ln\{\phi(\xi)\}$, the cumulant generating function, about the origin, where $\phi(\xi)$ is the characteristic function

$$\phi(\xi) = \sum_r p_r e^{i\xi Y_r}.$$

Some of the properties of $\mathrm{cum}(Y_1, \ldots, Y_r)$ are:

i. If $(Y_1, \ldots, Y_r)$ can be divided into two or more groups independent of each other then $\mathrm{cum}(Y_1, \ldots, Y_r) = 0$

ii. If $(Y_1, \ldots, Y_r)$ and $(Z_1, \ldots, Z_r)$ are independent, then $\text{cum}(Y_1+Z_1, \ldots, Y_r+Z_r) = \text{cum}(Y_1, \ldots, Y_r) + \text{cum}(Z_1, \ldots, Z_r)$

iii. $\text{cum}Y_j = E[Y_j]$ for $j = 1, \ldots, r$

Here $E[\cdot]$ denotes the expected value.

If the series $\mathbf{X}(t)$ is stationary up to order k, we define the second order spectrum of the sub-series $X_a(t)$ with the sub-series $X_b(t)$ as

$$f_{ab}(\omega) = \sum_{u=-\infty}^{\infty} c_{ab}(u)e^{-i\omega u}, \tag{5.1}$$

where $c_{ab}(u) = c_{ab}(t+u, t)$ [7]. $f_{ab}(\omega)$ is called the cross-spectrum. When $a = b$ it is just the power spectrum $P(\omega)$.

All this can be extended to the kth order and we get a kth order cumulant spectrum, $f_{a_1,\ldots,a_k}(\omega_1, \ldots, \omega_{k-1})$:

$$f_{a_1,\ldots,a_k}(\omega_1, \ldots, \omega_{k-1}) = \sum_{u_1,\ldots,u_{k-1}}^{\infty} c_{a_1,\ldots,a_k}(u_1, \ldots, u_{k-1}) \exp\left\{-i\sum_{j=1}^{k-1} u_j\omega_j\right\}$$

for $-\infty < \omega_j < \infty$, $a_1, \ldots, a_k = 1, \ldots, r$, $k = 2, 3 \ldots$. Since when the series $\mathbf{X}(t)$ is stationary,

$$c_{a_1,\ldots,a_k}(t_1 + u, \ldots, t_k + u) = c_{a_1,\ldots,a_k}(t_1, \ldots, t_k),$$

we can remove this redundancy by using the notation [7]

$$c_{a_1,\ldots,a_k}(t_1, \ldots, t_{k-1}).$$

A cumulant spectrum of order 3 is called a bispectrum B_X:

$$B_X(\omega_1, \omega_2) = \sum_{u_1,u_2=-\infty}^{\infty} c_X(u_1, u_2)e^{-i(u_1\omega_1+u_2\omega_2)}$$

with $c_X(u_1, u_2) = E[X(t)X(t+u_1)X(t+u_2)]$. The bispectrum can also be written as [8]

$$B_X(\omega_1, \omega_2) = E[\hat{X}(\omega_1)\hat{X}(\omega_2)\hat{X}^*(\omega_1 + \omega_2)]$$

where $\hat{X}$ denotes the Fourier transform of X and the asterisk the complex conjugate. This shows how the bispectrum estimates the statistical dependence between three waves. If the waves present at ω_1, ω_2 and $\omega_1 + \omega_2$ are uncorrelated with three different phases randomly distributed over $(-\pi, \pi)$, the averaging will cause the bispectrum to vanish [8]. If the waves are linearly coupled, however, the phases will not be random and the averaging

will not result in a zero value of the bispectrum. This also follows from the property $i.$ in the list of properties of the cumulants above.

To compensate for the different amplitudes in the spectra for different frequencies and thus get a quantitative measure of the phase coherence between the waves, one can make use of the bicoherence spectrum, which is basically the bispectrum normalised by the auto-power spectrum [9]:

$$b(\omega_1, \omega_2) = \frac{|B(\omega_1, \omega_2)|}{\sqrt{P(\omega_1)P(\omega_2)P(\omega_1 + \omega_2)}}. \tag{5.2}$$

Using Schwartz' inequality, one can show [10] that the bicoherence spectrum is bounded by $0 \leq b \leq 1$.

5.1.1 A Numerical Example of Bicoherence

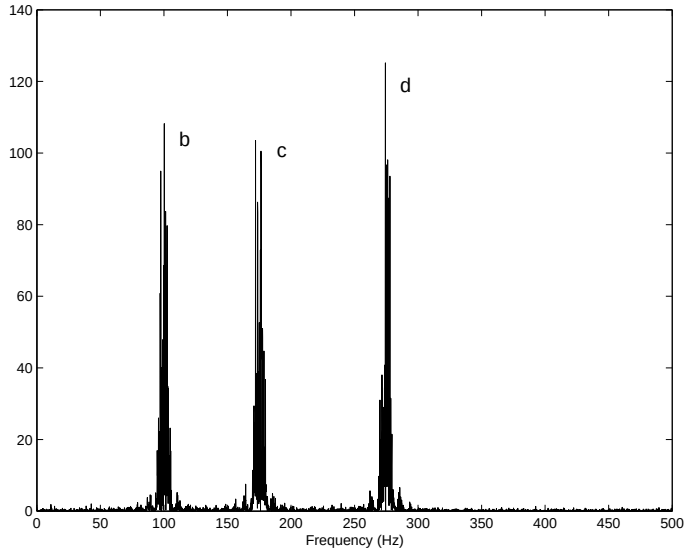

FIGURE 5.1: *The power spectrum of the test signal $X(t)$ in equation (5.3) containing three waves with phases that satisfy $\theta_d = \theta_b + \theta_c$ and added noise.*

To test the theory presented above, a test signal was created as follows (the steps are more or less the same as in [8]):

i. A set of 64 data records, each consisting of 128 data points was created, using the test signal

$$X(t) = \cos(\omega_b t + \theta_b) + \cos(\omega_c t + \theta_c) + \cos(\omega_d t + \theta_d) + g(t) \tag{5.3}$$

where $g(t)$ is added noise.

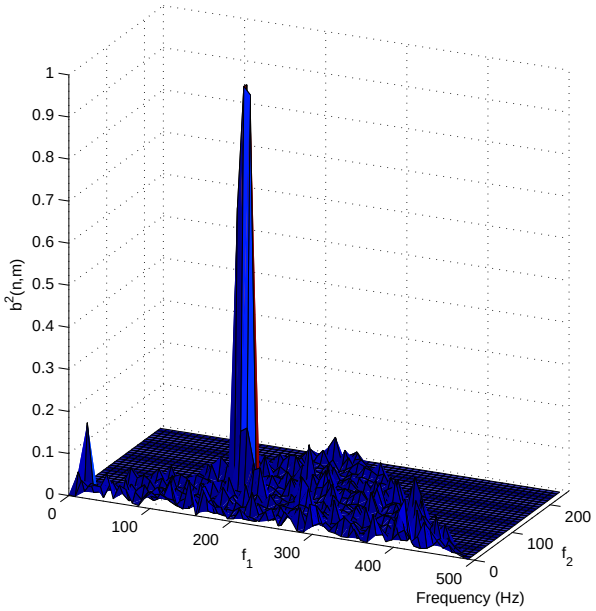

FIGURE 5.2: *The squared bicoherence spectrum of three waves with phases that satisfy* $\theta_d = \theta_b + \theta_c$ *and added noise. The power spectrum is shown in figure 5.1.*

ii. The mean value was subtracted from each record.

iii. The Hamming data window was applied to each record to reduce spectral leakage [6]. See section 5.3 for an introduction to windows and appendix A.1 for the MATLAB code.

iv. The Fourier amplitudes was calculated, using the FFT technique [11]:

$$\hat{X}_n^{(i)} = \frac{1}{128} \sum_{t=1}^{128} X(t) e^{\frac{-i2\pi nt}{128}}$$

where $n = 1, \ldots, 128/2$ and $i = 1, \ldots, 64$. Note that t is the position in the vector of values, that is, not continuous time.

v. The bispectrum was calculated using

$$B(n,m) = \frac{1}{64} \sum_{i=1}^{64} \hat{X}_n^{(i)} \hat{X}_m^{(i)} \hat{X}_{n+m}^{*(i)}$$

Further, equation (5.2) was used to normalise the bispectrum. All this can rather easily be done in, for example, MATLAB (see appendix A.2 for the program code).

First, the frequencies of the three oscillators were chosen to be $f_b = 100$ Hz, $f_c = 175$ Hz and $f_d = f_b + f_c = 275$ Hz. The phases of oscillators b and c were with certain time intervals chosen randomly from $(-\pi, \pi)$. The third oscillator, d, was given the sum of the phases of oscillators b and c, that is, $\theta_d = \theta_b + \theta_c$. The power spectrum is shown in figure 5.1 and the squared bicoherence spectrum in figure 5.2. It can be seen that strong coherence exists between the waves at frequencies $f_b = 100$ Hz, $f_c = 175$ Hz and their sum frequency $f_d = 275$ Hz. This is due to the consistency of the phases of oscillators b, c and d. The bicoherence spectrum is limited by the region $0 \leq f_1 \leq \infty$, $0 \leq f_2 \leq f_1$ [12].

Next, the phase of the d-wave was also chosen from a set of random numbers distributed over $(-\pi, \pi)$. The power spectrum of this signal is shown in figure 5.3. It is evident that this power spectrum is very similar to the power spectrum in figure 5.1; no difference can be seen, except for the amplitude differences due to noise. It is obvious that the power spectrum is unable to tell anything about the phase coherence due to any nonlinearities. The bicoherence spectrum in figure 5.4, on the other hand, clearly shows the lack of crrelation between the waves, since no peak at the sum frequency is present.

Note that constant phases of all three oscillators with $\theta_b + \theta_c \neq \theta_d$ will produce a peak at the sum frequency, since there is still correlation between the waves (the phases are separated equally at all time). Also, the phase must not be changed too often, since this will "destroy" the wave.

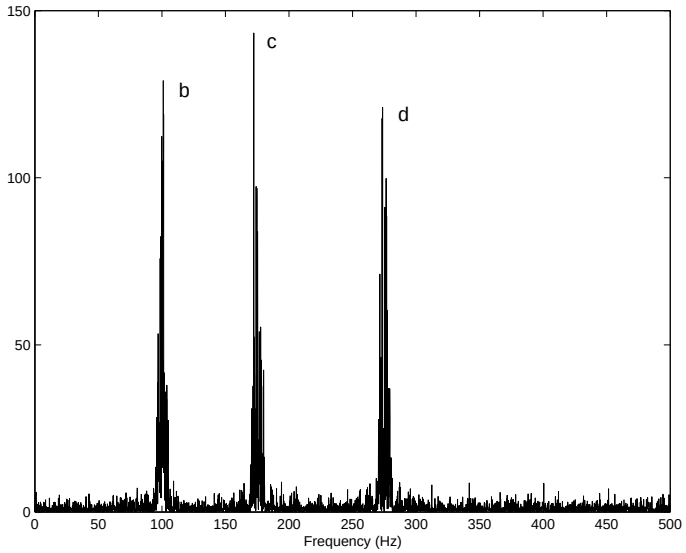

FIGURE 5.3: *The power spectrum of the test signal $X(t)$ in equation (5.3) containing three waves with independent phases.*

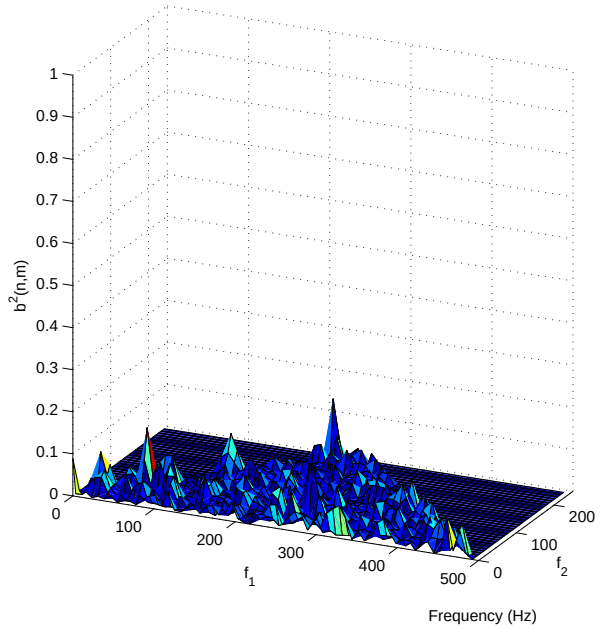

FIGURE 5.4: *The squared bicoherence spectrum of three waves with independent phases and added noise. The power spectrum is shown in figure 5.3*

Next, a product term was inserted, giving the following test signal, with θ_b, θ_c and θ_d independent:

$$\begin{aligned} X(t) = &\cos(\omega_b t + \theta_b) + \cos(\omega_c t + \theta_c) + \frac{1}{2}\cos(\omega_d t + \theta_d) \\ &+ \cos(\omega_c t + \theta_c)\cos(\omega_b t + \theta_b) + g(t) \end{aligned} \tag{5.4}$$

The product term can be rewritten as

$$\begin{aligned} &\cos(\omega_c t + \theta_c)\cos(\omega_b t + \theta_b) \\ &= \frac{1}{2}\left\{\cos[(\omega_c - \omega_b)t + \theta_c - \theta_b] + \cos[(\omega_c + \omega_b)t + \theta_c + \theta_b]\right\} \\ &= \frac{1}{2}\left\{\cos(\omega_a t + \theta_a) + \cos(w_d t + \theta_d)\right\} \end{aligned}$$

where $\omega_a = \omega_c - \omega_b$ and $\theta_a = \theta_c - \theta_b$.

As can be seen, the product produces a new wave with frequency $f_a = f_c - f_b$. The result can be seen in figures 5.5 and 5.6. A new wave, a, at the difference frequency between c and b is seen. At $f_d = f_b + f_c$, a peak of approximately half the height of the peak in figure 5.2 is present. Since the phase of d is uncorrelated to b and c, the peak must be due to the product

interaction. Thus half the power at f_d is due to product interaction and the other half independent of this interaction. The new peak at $f_a = f_c - f_b$ is entirely due to the product interaction. From the power spectrum alone in figure 5.5 it is impossible to tell if the waves at f_a and f_d are generated by interaction of the waves at f_b and f_c.

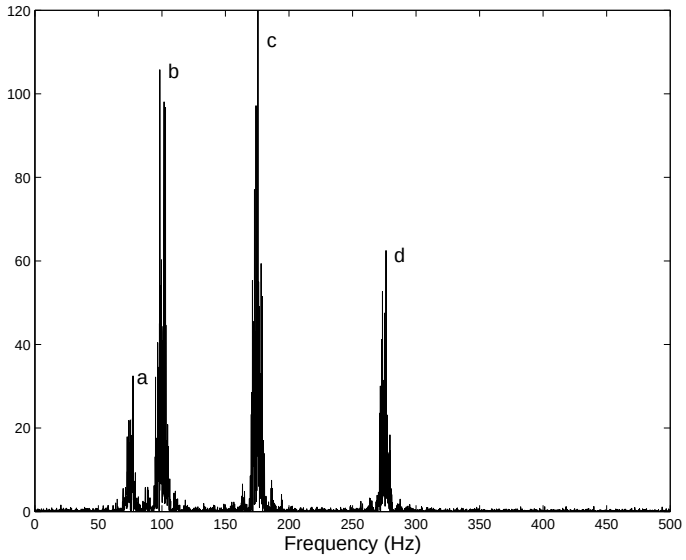

FIGURE 5.5: *The power spectrum of the test signal $X(t)$ in equation (5.4) containing four waves with θ_b, θ_c and θ_d independent, quadratic coupling of two waves and added noise.*

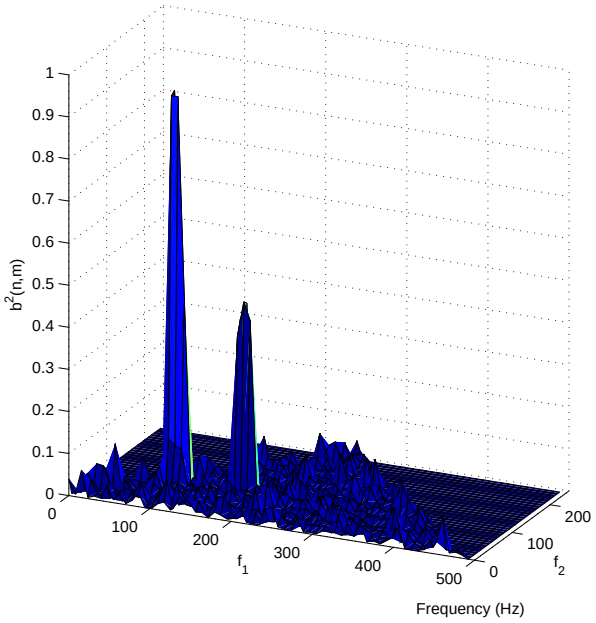

FIGURE 5.6: *The squared bicoherence spectrum of the test signal $X(t)$ in equation (5.4) containing four waves with θ_b, θ_c and θ_d independent, quadratic coupling of two waves and added noise. The power spectrum is shown in figure 5.5.*

5.2 Autocorrelation and Cross-correlation

As shown in equation (5.1), the Fourier transform of the second order cumulant gives the power spectrum or the cross-spectrum. It is, however, possible to use the second order cumulants directly as an analysis tool. The autocorrelation and cross-correlation, the second order cumulants, are built on the covariance function $C_{XX} = E[(X - \mu_X)(Y - \mu_Y)]$, where $\mu_X = E[X] = \frac{1}{N}\sum_{n=1}^{N} X_n$. The auto-covariance sequence of a time series is defined as

$$R_{XX}(m) = E[\{X_{n+m} - \mu_X\}\{X_n^* - \mu_X\}]$$

As seen from the equation above, it multiplies the value of the auto-covariance at position $n+m$ (with the mean subtracted) with the complex conjugate of the value at position n (with the mean subtracted) through the whole series, sums the terms for equal shift m and then makes a mean of the terms. The shift m is often called the lag and runs from 0 to $N-1$, where N is the length of the series. Thus, if the signal is random, on average the terms in the auto-covariance function for a certain m sum up to zero, except for $m = 0$ when the value at position n is multiplied with the complex conjugate of itself.

The autocorrelation function is then:

$$\rho_{XX}(m) = \frac{R_{XX}(m)}{R_{XX}(0)}. \tag{5.5}$$

This function has a maximal value of 1 (at maximum correlation), $\rho_{XX}(m) \leq 1$, for all m. Usually, autocorrelation is performed in the time domain, but in this work it is performed in the frequency domain. In conventional terminology, this is called the auto-coherence [13, 14][1].

In many cases it is more useful to use the cross-correlation, for example when correlating two separate parts of the same spectrum. The cross-covariance function is defined as

$$R_{XY}(m) = E[\{X_{n+m} - \mu_X\}\{Y_n^* - \mu_Y\}]$$

where $\mu_X = E[X]$ and $\mu_Y = E[Y]$. The cross-correlation function is defined as

$$\rho_{XY}(m) = \frac{R_{XY}(m)}{(R_{XX}(0)R_{YY}(0))^{1/2}}. \tag{5.6}$$

The cross-correlation function also has a maximal value of 1 (at maxium correlation), but differs from the autocorrelation function since the autocorrelation always produces a peak of height 1 at zero lag ($m = 0$). This is because the cross-correlation function is the "auto-correlation" function of

[1] There seems to be a confusion in some articles regarding the terminology in spectral analysis. Equation (5.5) is in some articles referred to as auto-coherence and in other articles as auto-coherence, which should be something else.

two separate series which need not be equal at $m = 0$. Further, the autocorrelation function is also symmetric about zero, whereas the cross-correlation function most often is not.

In MATLAB, the cross-correlation function is defined as

$$R_{XY}(m) = E[X_{n+m}Y_n^*].$$

The function `xcorr` then provides a normalisation `'coeff'`, that corresponds to the correlation functions 5.5 and 5.6, except for the subtraction of the means (see also [15]).

5.2.1 A Numerical Example of Autocorrelation in the Frequency Domain

To test the autocorrelation in the frequency domain, the test signal (5.3), except the frequency sum term, was reproduced:

$$X(t) = \cos(\omega_b t + \theta_b) + \cos(\omega_c t + \theta_c) + g(t) \tag{5.7}$$

Then this signal was Fourier transformed. The results are shown in figures 5.7, 5.8, 5.9 and 5.10. Figure 5.7 shows the power spectrum of the testsignal $X(t)$ in equation (5.7 when the phases of the two oscillators are the same. The corresponding autocorrelation plot is shown in figure 5.8, where a peak at lag corresponding to 75 Hz is seen, which is the frequency separation of the two oscillators. This suggests that a correlation exists between the waves. Next, the second oscillator was given a phase independent of the phase of the first oscillator. The power spectrum is shown in figure 5.9 and the autocorrelation plot in figure 5.10. As can be seen, no correlation is indicated. It is impossible to tell from the two power spectra in figures 5.7 and 5.9 whether they contain correlated waves or not.

5.3 Windows

In section 5.1.1, where the bicoherence was tested, a data window was applied to the signal to reduce spectral leakage. This spectral leakage phenomenon arises because of the finite length of the time series available. This section begins with the Dirichlet kernel, who is the villain of the piece, and then discusses the use of data windows, especially the Hamming window used in this work, to reduce the effect of the Dirichlet kernel.

5.3.1 The Dirichlet Kernel

The Dirichlet kernel appears when an infinite time series is truncated and Fourier transformed. The Fourier transform of a time series $X(t)$ is defined

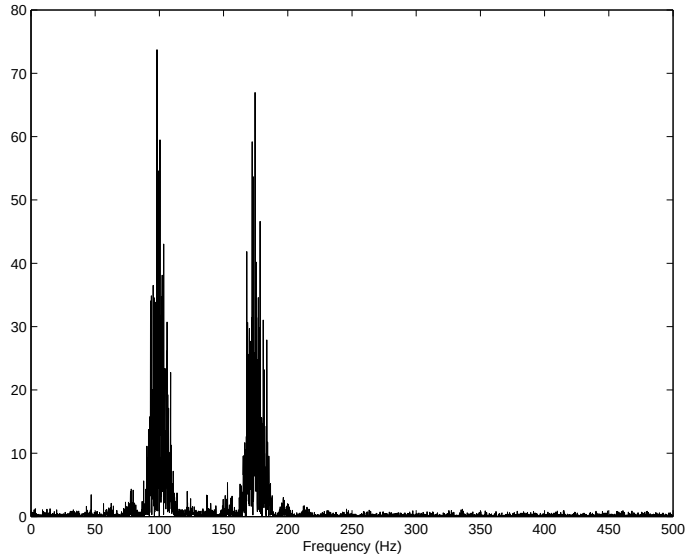

FIGURE 5.7: *Power spectrum of the test signal $X(t)$ in equation (5.7) containing two waves with equal phases at frequencies 100 Hz and 175 Hz and with added noise.*

as

$$\hat{X}(\omega_k) = \sum_{n=1}^{N-1} X(t_n) e^{-i\omega_k t_n}, \ k = 1, 2, \ldots, N-1$$

and its inverse by

$$X(t_n) = \frac{1}{N} \sum_{k=1}^{N-1} \hat{X}(\omega_k) e^{i\omega_k t_n}, \ n = 1, 2, \ldots, N-1$$

where $i = \sqrt{-1}$.

Common sense says that time series cannot be infinite. However, the finite time series can be seen as a part of an infinite time series. This then corresponds to multiplying the infinite time series by a rectangular window, a window function, that is unity on our observation interval and zero elsewhere:

$$w(n) = 1.0, \ n = 0, 1, 2, \ldots, N-1.$$

Multiplication in the time domain is equal to convolution in the frequency domain, so the Fourier transform of the original infinite time series is convolved with the Fourier transform of the window function $w(n)$. The Fourier transform of $w(n)$ is

$$W(\omega) = \exp\left(-i\frac{N-1}{2}\omega\right) \frac{\sin\left(\frac{N}{2}\omega\right)}{\sin\left(\frac{1}{2}\omega\right)}. \tag{5.8}$$

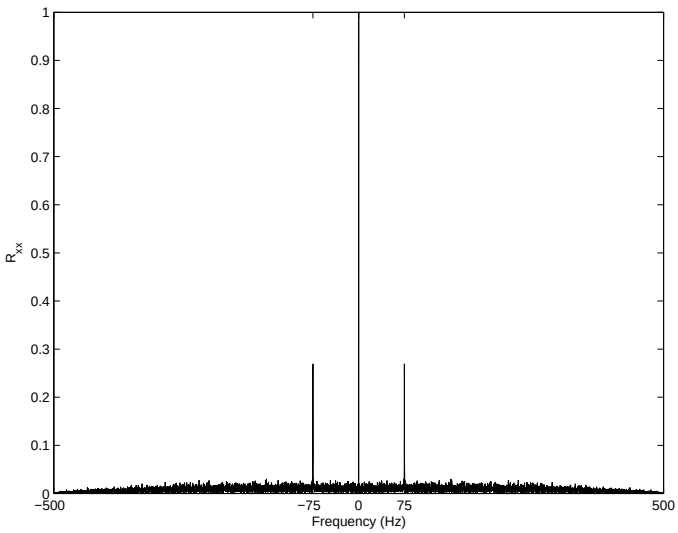

FIGURE 5.8: *Normalised autocorrelation of the test signal $X(t)$ in equation (5.7) containing two waves with equal phases, separated by 75 Hz and with added noise.*

This is known as the Dirichlet kernel and can be seen in figure 5.11. So, the transform of the truncated series $X(\omega_k)$ will be a distorted version of the transform of the infinite series $X_o(\omega_k)$.

The width of the main lobe of the Dirichlet kernel will smooth out peaks in the power spectrum of the signal. If two peaks are located closer to each other than the width of the main lobe, the kernel may fail to resolve the two peaks and only detect one peak. Increasing N in equation 5.8 will narrow the main lobe, making it possible to resolve the peaks. The width of the main lobe is usually taken as the width at 3 dB below the main lobe peak.

5.3.2 The use of Windows

Because of the side lobes of the Dirichlet kernel, contribution to, say, $X(\omega_0)$ will not only come from ω_0 but also from other ω where the amplitude is not zero. This phenomenon is called spectral leakage; power from neighbouring frequencies "leak" to the central frequency as shown in figure 5.12. At the top row in the figure, the Dirichlet kernel is shown to the left and the spectrum to be examined to the right. Multiplying these two, as shown in the lower left part of the figure, contribution to ω_0 comes also from the side lobes (shaded areas) and the result is seen in the lower right corner, where the resulting spectral line at ω_0 has contribution from the shaded areas to the left. Spectral leakage is not desirable, so another window is applied to attenuate the side lobes of the Dirichlet kernel. There are many windows

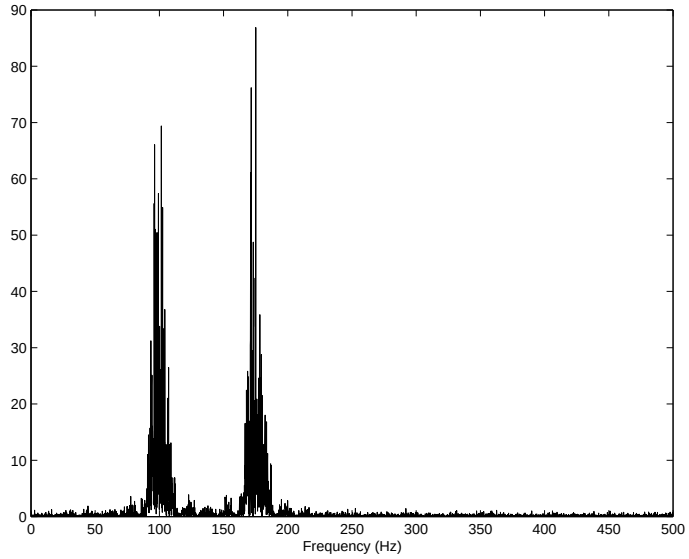

FIGURE 5.9: *Power spectrum of the test signal $X(t)$ in equation (5.7) containing two waves with phases at frequencies 100 Hz and 175 Hz and with added noise.*

with different characteristics available (see [16] for a nice review of windows). The equation of the Hamming window is

$$0.54 - 0.46 \cos\left(\frac{2\pi}{N} n\right), \ n = 0, 1, 2, \ldots, N-1.$$

The coefficients 0.54 and 0.46 are nearly the ones that achieve minimum sidelobe levels [16]. This window is also easy to implement and has a relatively narrow main lobe. The Hamming window used in this work can be seen in figure 5.13.

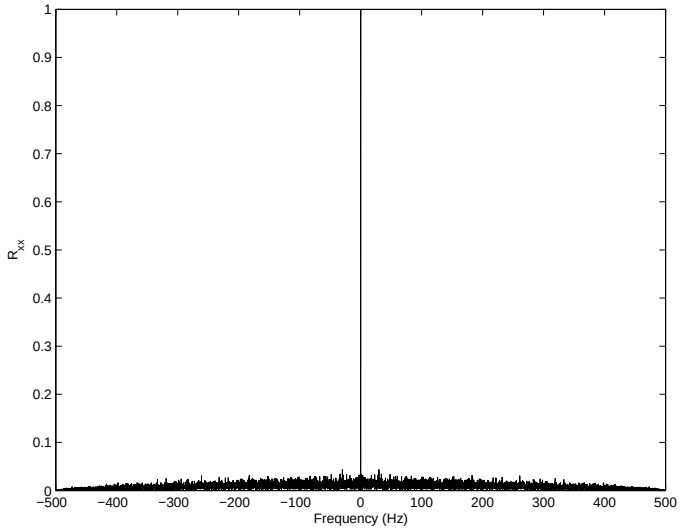

FIGURE 5.10: *Normalised autocorrelation of the test signal $X(t)$ in equation (5.7) containing two waves with independent phases, separated by 75 Hz and with added noise.*

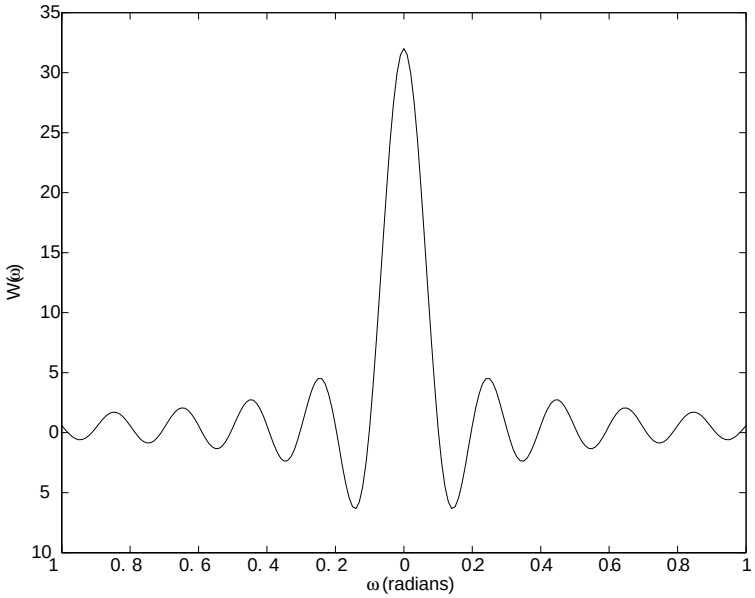

FIGURE 5.11: *The Dirichlet kernel. The coordinates are normalised with sample period $T = 1.0$, so that $W(\omega)$ has the period 2π.*

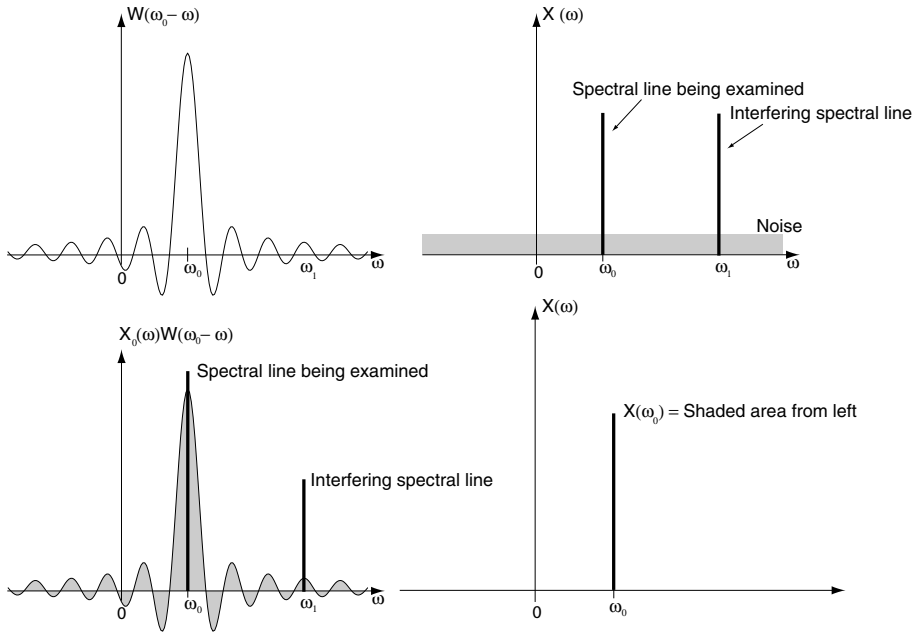

FIGURE 5.12: *The effect of the Dirichlet kernel. Contribution to* $X(\omega_0)$ *comes from other* ω *as well as from* ω_0.

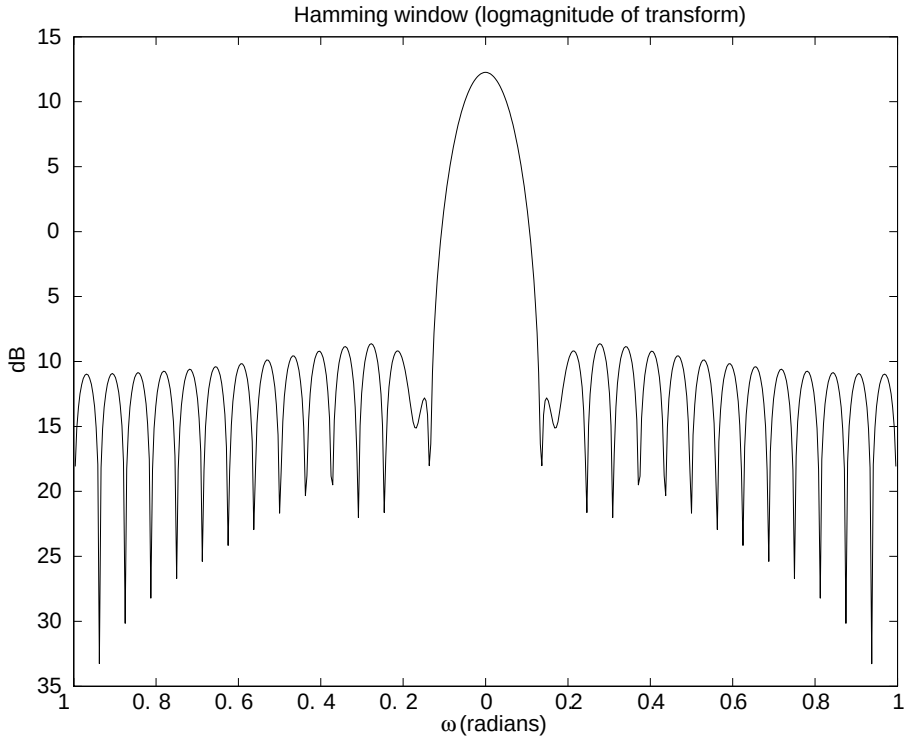

FIGURE 5.13: *The Hamming window. The coordinates are normalised with sample period* $T = 1.0$*, so that* $W(\omega)$ *has the period* 2π.

Chapter 6

Spectral Analysis

In this work, data from experiments at the Sura facility near Nizhny Novgorod, Russia, in 1998 and at the EISCAT–Heating facility near Tromsø, Norway, in 1999 have been analysed.

When using continuous wave pumping of the ionospheric plasma, that is, when not turning the pump wave on and off with defined intervals, a stable process which can be considered to be stationary can be obtained. Here such stationary conditions are considered.

Unfortunately, radiation at the sum and difference frequencies (of, for example, the DM and 2DM) could not be detected on the ground, making it impossible to carry out the bicoherence analysis. Autocorrelation in the frequency domain is on the other hand possible to perform. It will not, as the bicoherence, detect which two waves that interact to give the third wave or indicate the correlation that exists between the three waves in, for example, the test signal equation 5.3. It will instead detect the correlation between wave b and c, b and d and c and d separately in the same equation.

To do the autocorrelation, the complex time series from the SEE measurements was divided into several smaller windows and then combined to a matrix. Each window was tapered with the Hamming window and Fourier transformed with the fast Fourier transform algorithm that comes with MATLAB using as many points as there were in each window, that is, without zero padding. A short program was written in MATLAB (see appendix A.2) to perform the autocorrelation with the MATLAB signal processing toolbox algorithm `xcorr` [15].

Another method applied was cross-correlation (see, for example, [15] or [17]) of different parts of the same SEE spectrum. This has the advantage of that parts of the spectrum separated by some spectral feature can be correlated without the interference of the spectral feature between them. As an example the DM and the BUM can be correlated without the strong interference of the pump wave. The data was processed in a similar manner as when performing the autocorrelation.

The shortest Hamming windows consisted of 1000 to 1024 points. With a sampling frequency of 320 kHz this gives a resolution of the window (width of main lobe at -3 dB) of 0.392 kHz, which is sufficient for the spectral features in the SEE data. This particular window was chosen because of its ease of implementation, relatively small side lobes and good frequency resolution (see [16]).

Chapter 7

Results and Discussion

In this chapter the results from the cross-correlation analyses are presented. By comparing the results with analyses of a test signal containing white noise it was found that the spectral features in the SEE spectra are very noise-like, no matter what feature analysed. It was also seen that the standard deviation of the cross-correlation remained constant when the number of points in the mean was increased, which is the same result obtained when doing the same analysis on white noise.

7.1 Results

The cross-correlation between different parts of the spectrum was found to be the most useful tool, since widely separated parts can be correlated without the interference of the spectrum in between. The autocorrelation analyses, giving no results worthy a discussion, will therefore be omitted. A test signal containing white noise was created to see how the cross-correlation of such a signal would look like. The result can be seen in figure 7.1 where the cross-correlation function has a pyramidal shape. This must not be interpreted as maximum correlation at lag zero, because the cross-correlation is biased due to the decreasing number of data points in the correlation at higher lags. As discussed in section 5.2, the lag m runs from 0 to $N-1$, where N is the length of the series (in this case the length of the windows). As m increases fewer and fewer terms are included in the sum, till m reaches $N-1$, when only one term can be included in the sum and that is the multiplication of the two values at each end of the series. No more terms exist for which the separation between the two is $N-1$.

Comparing[1] the cross-correlation of the white noise with the cross-correlation of the signals from the SEE data, it is seen that they are very similar.

[1] The vertical lines in the spectra show the intervals which have been correlated and the corresponding label tells where the interval starts and stops. Δf is the width of the windows.

Figure 7.2 shows the cross-correlation of parts of the spectrum for sura98_238 where there should be no correlation. It is indeed very similar to the cross-correlation of white noise in figure 7.1. Figure 7.4 shows a cross-correlation within the BUM in the same spectrum, which also is reminiscent of the cross-correlation of white noise. Analyses within the BUM have been done in files sura98_239, sura98_240, sura98_260 and trom99_583, all with results equivalent to figure 7.4. Figure 7.6 shows cross-correlation between the DM and upshifted maximum (UM), which again is similar to the previous cross-correlations. This is a mean of only 52 windows because of the short original signal in sura98_240. The same spectral features have also been analysed in files sura98_239 and trom99_583, giving the same results. A cross-correlation between the DM and BUM is shown in figure 7.8 and between the 2DM and DM in figure 7.10. The DM and BUM have also been cross-correlated with the same results in files sura98_239, sura98_240 and trom99_523, and the 2DM and DM with the same result in sura98_313. Thus, the cross-correlation analysis suggests that the studied SEE data from the Sura 1998 and Tromsø 1999 experiments are noise-like. The resulting radiation from the electromagnetically driven plasma turbulence at the location of detection on the ground is incoherent.

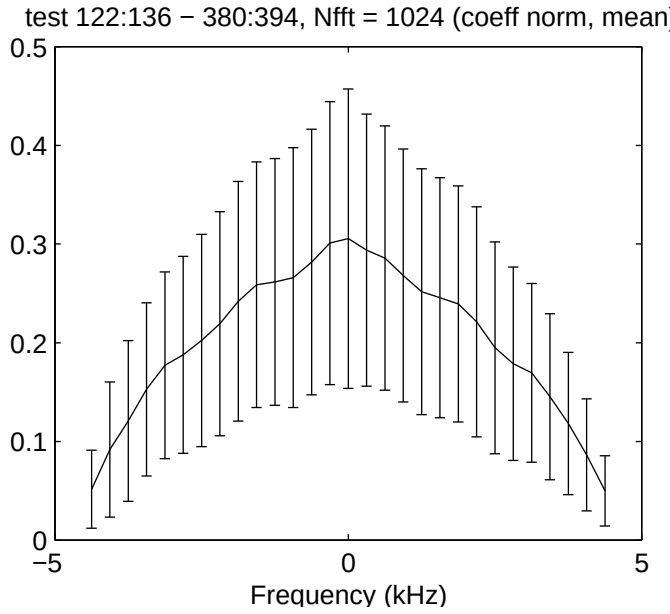

FIGURE 7.1: *Cross-correlation with standard deviation of two separate parts of a spectrum containing white noise. Mean of 400 windows.*

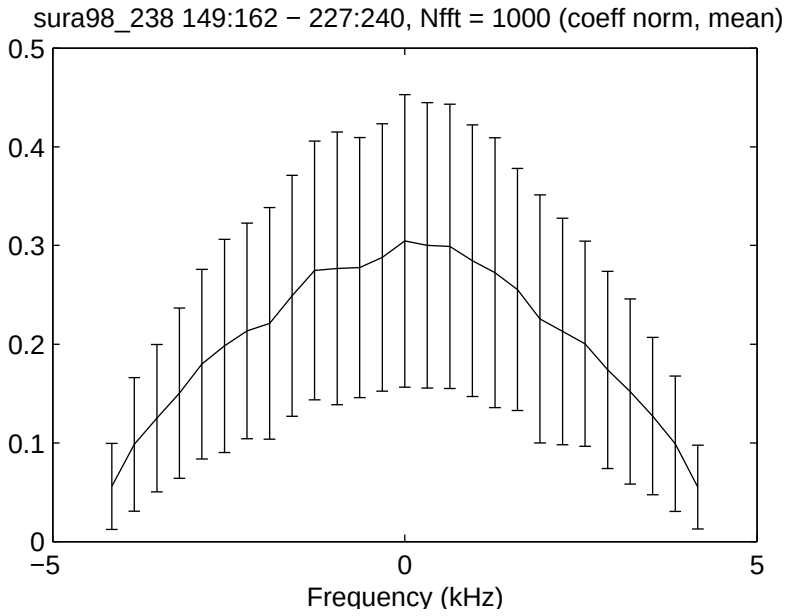

FIGURE 7.2: *Cross-correlation of parts of the spectrum where there should be no correlation (sura98_238). Mean of 400 windows. See figure 7.3 for spectrum.*

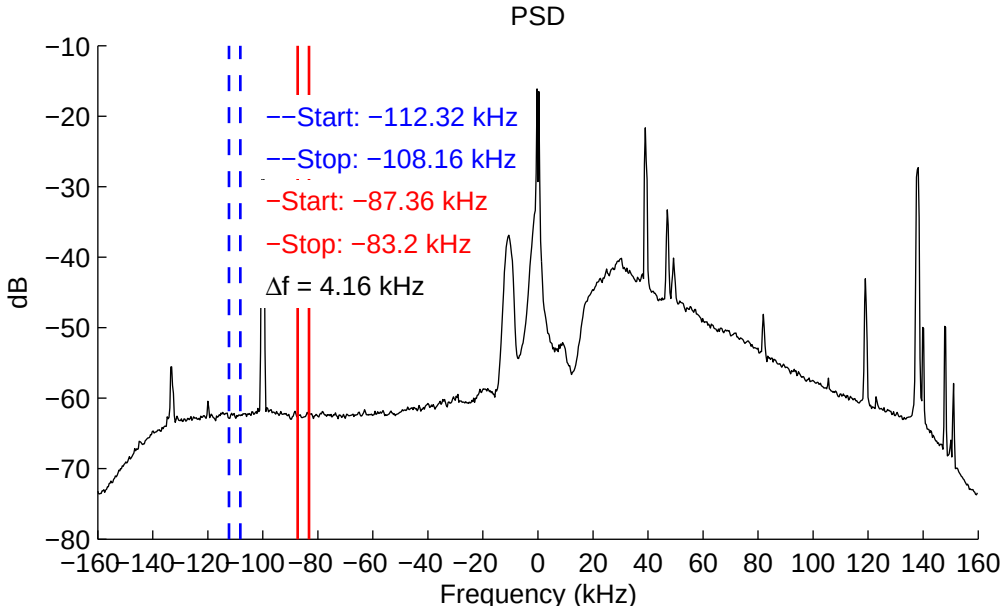

FIGURE 7.3: *Spectrum for sura98_238.*

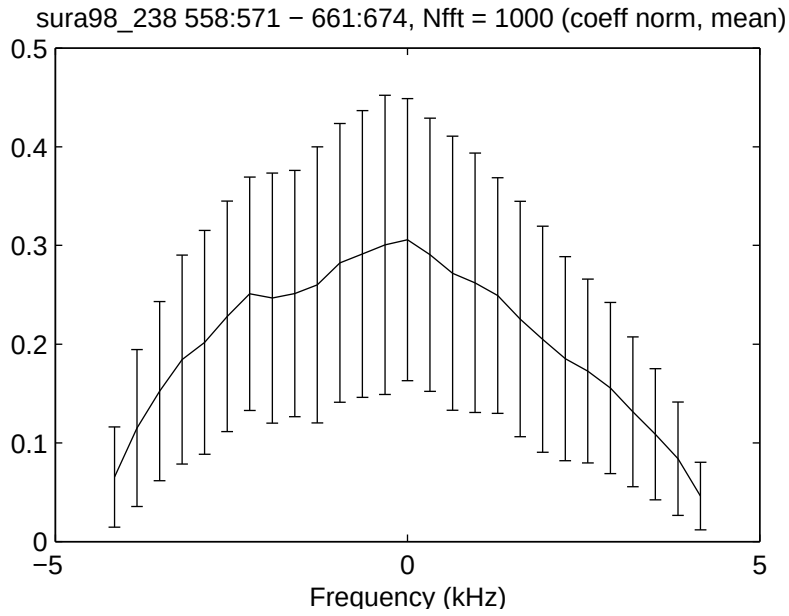

FIGURE 7.4: *Cross-correlation within the BUM (sura98_238). Mean of 400 windows. See figure 7.5 for spectrum.*

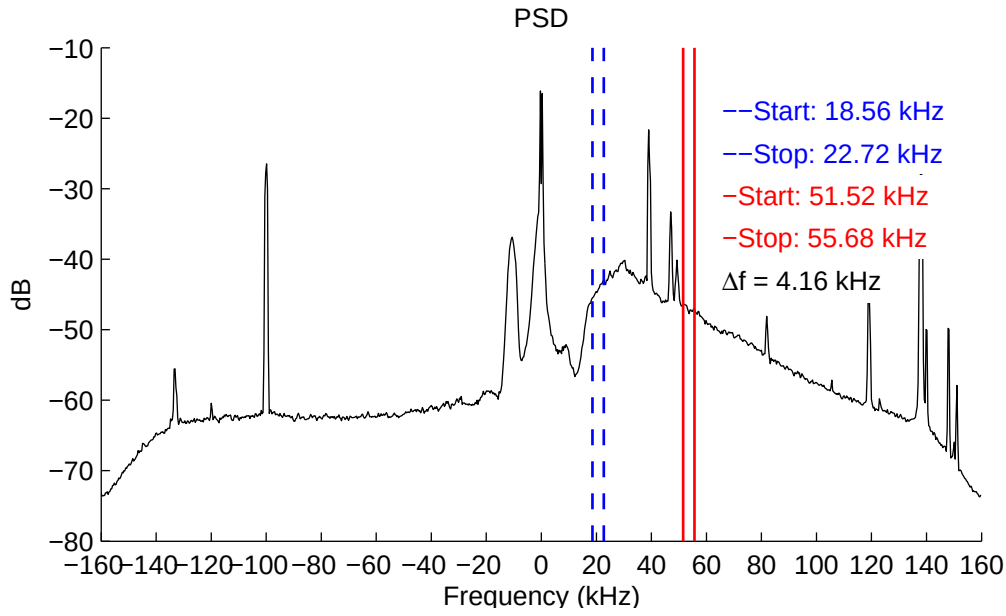

FIGURE 7.5: *Spectrum for sura98_238.*

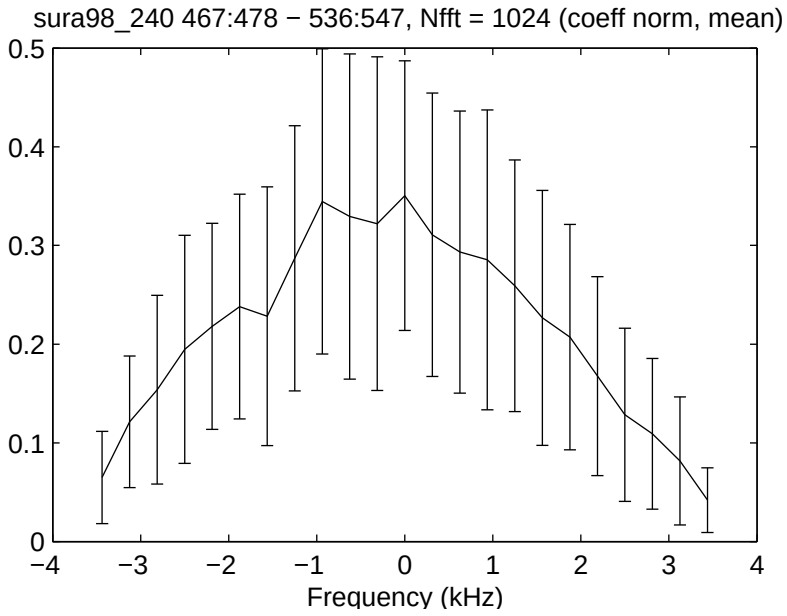

FIGURE 7.6: *Cross-correlation between the DM and the UM (sura98_240). Mean of 52 windows. See figure 7.7 for spectrum.*

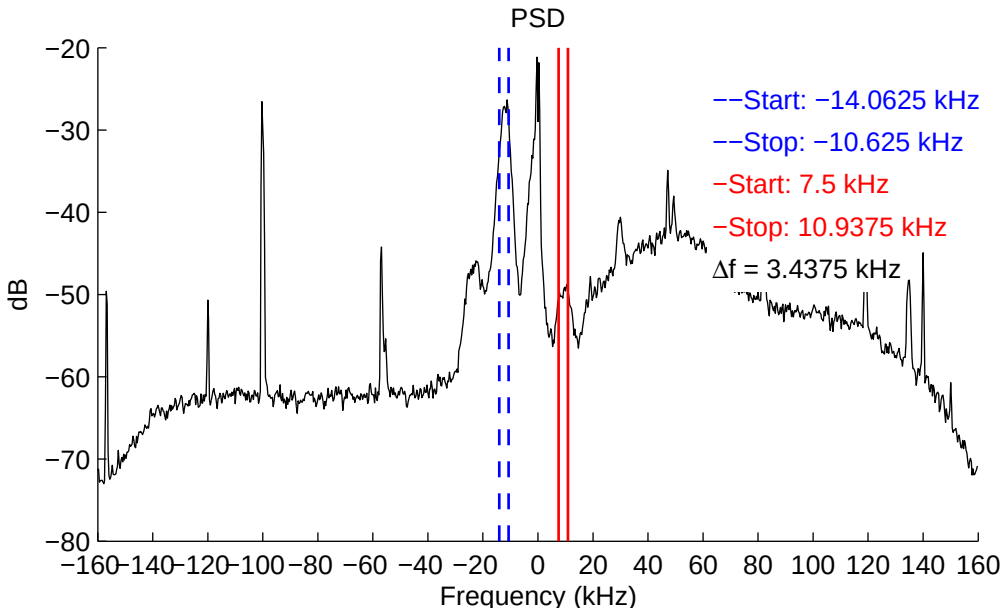

FIGURE 7.7: *Spectrum for sura98_240.*

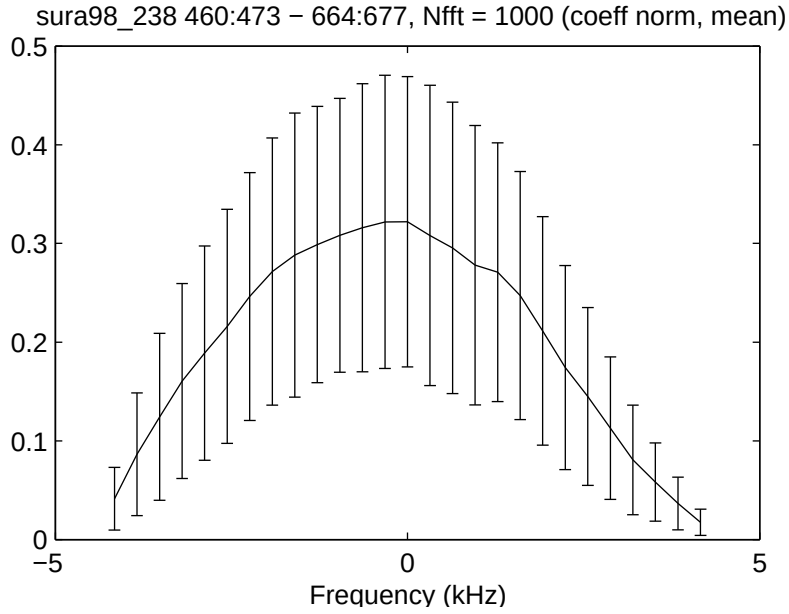

FIGURE 7.8: *Cross-correlation of the DM with BUM, (sura98_238). Mean of 400 windows. See figure 7.9 for spectrum.*

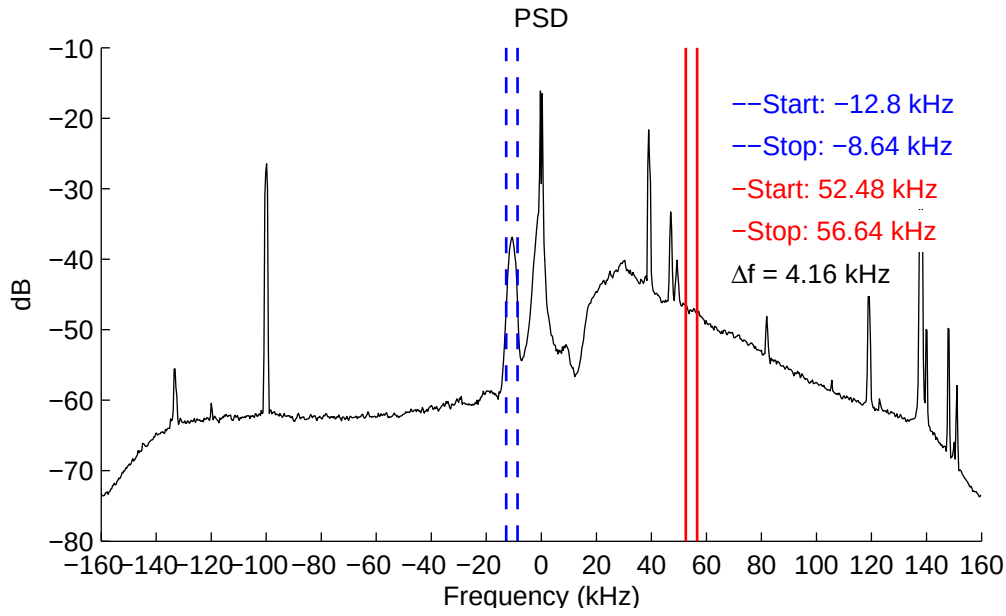

FIGURE 7.9: *Spectrum for sura98_238.*

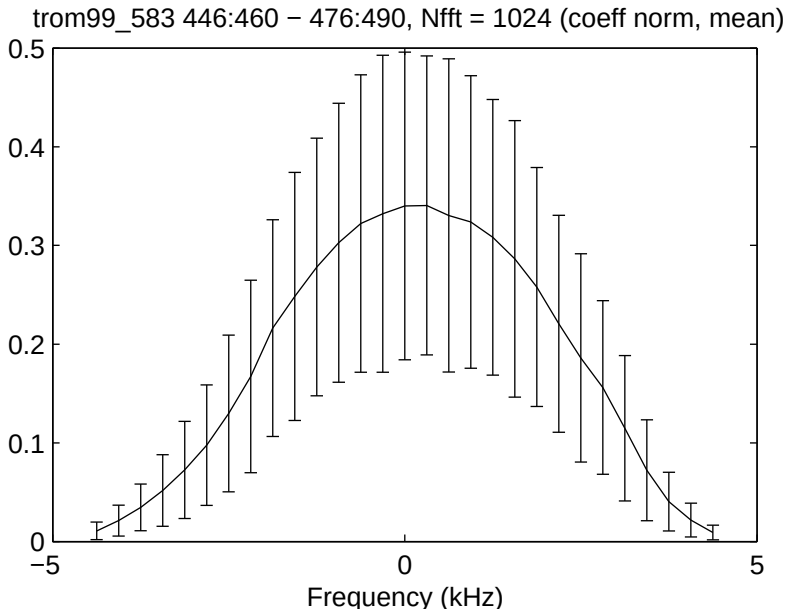

FIGURE 7.10: *Cross-correlation between the 2DM and DM (trom99_583). Mean of 400 windows. See figure 7.11 for spectrum.*

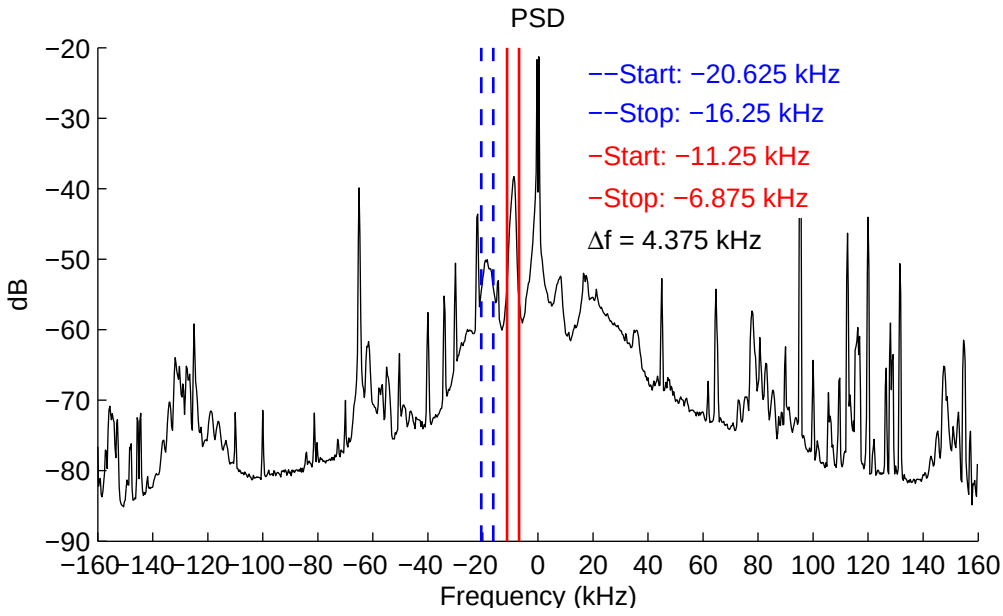

FIGURE 7.11: *Spectrum for trom99_583.*

Increasing the window length gives more data points and higher resolution and the peak value of the cross-correlation decreases. Figure 7.12 shows cross-correlation within the broad continuum (BC) in file trom99_520 with a window length of 1024. Again, it is very similar to the previous ones. In figure 7.14, the window length is increased to 4096, giving a resolution of less than 100 Hz. The peak value of the correlation as well as the standard deviation has decreased, which is expected, since the correlation is based on more data points. The window length is increased to 8192 in figure 7.16. No new prominent features can be seen. The peak value and standard deviation has decreased further.

Figure 7.4 is a mean of 400 windows and 7.18 is a mean of 1600 windows of the same file (sura98_238). Comparing these two, it is seen that the standard deviation is more or less constant. In figures 7.10 and 7.19 the 2DM and DM in file trom99_583 have been cross-correlated, the first figure containing a mean of 400 windows and the second a mean of 1600 windows. The differences in the figures are due to the extra data points included to get 1600 windows, keeping 1024 data points in each window. This is the same behaviour as with noise, as can be seen from figures 7.21, 7.1 and 7.22, all showing the cross-correlation of white noise. Figure 7.21 is a mean of 200 windows, figure 7.1 a mean of 400 windows. The last two figures do not differ much. Figure 7.22 is a mean of 1600 windows, showing a much smoother structure due to the enhanced statistics. Cross-correlations of other spectral features, such as within the BUM and between the DM and BUM, show the same behaviour when increasing the number of windows in the mean.

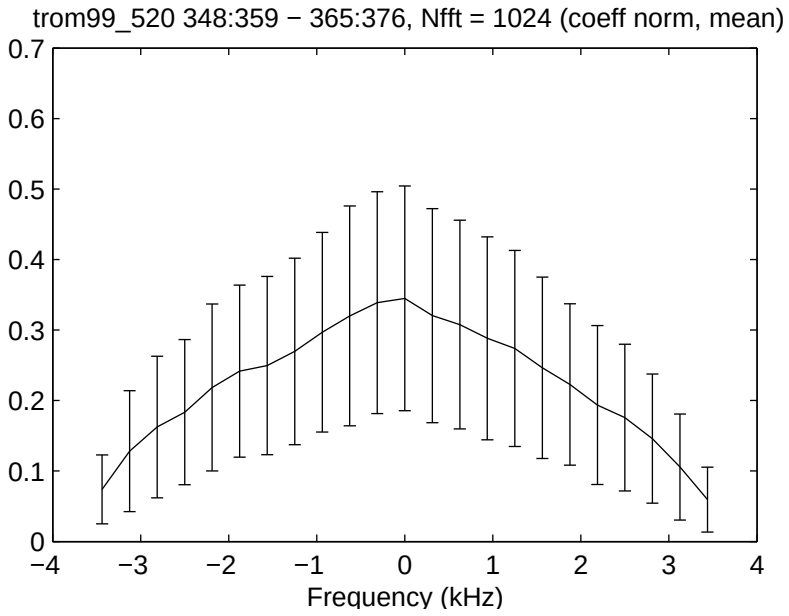

FIGURE 7.12: *Cross-correlation of the BC (trom99_520). Mean of 400 windows. See figure 7.13 for spectrum.*

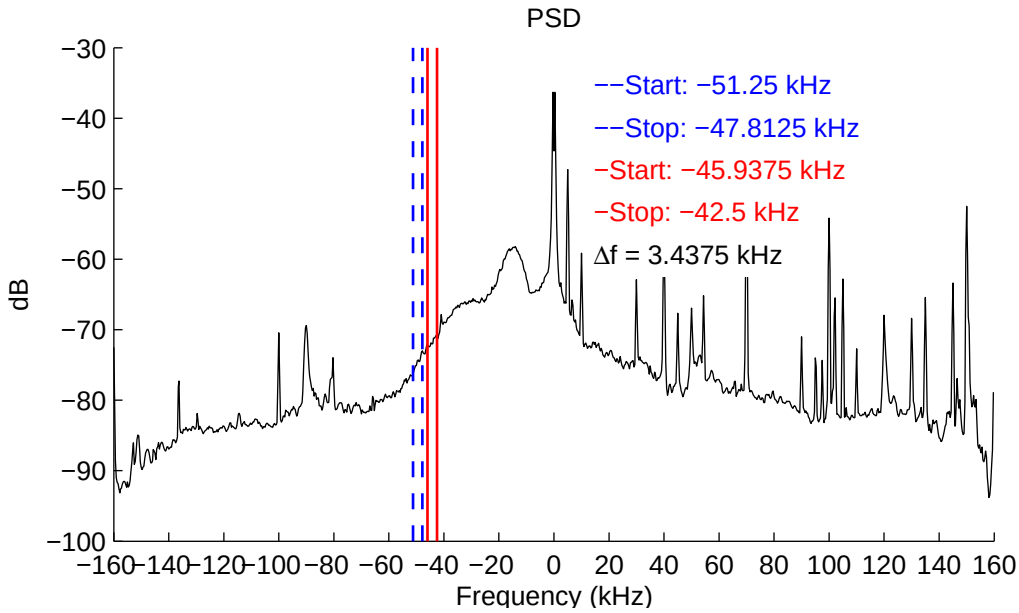

FIGURE 7.13: *Spectrum for trom99_520.*

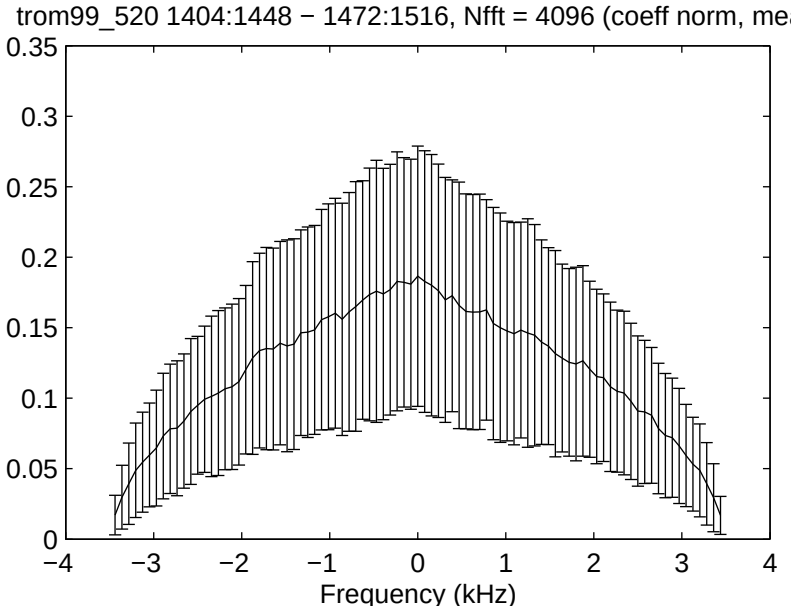

FIGURE 7.14: *Cross-correlation of the BC with 4096 data points per window (trom99_520). Mean of 400 windows. See figure 7.15 for spectrum.*

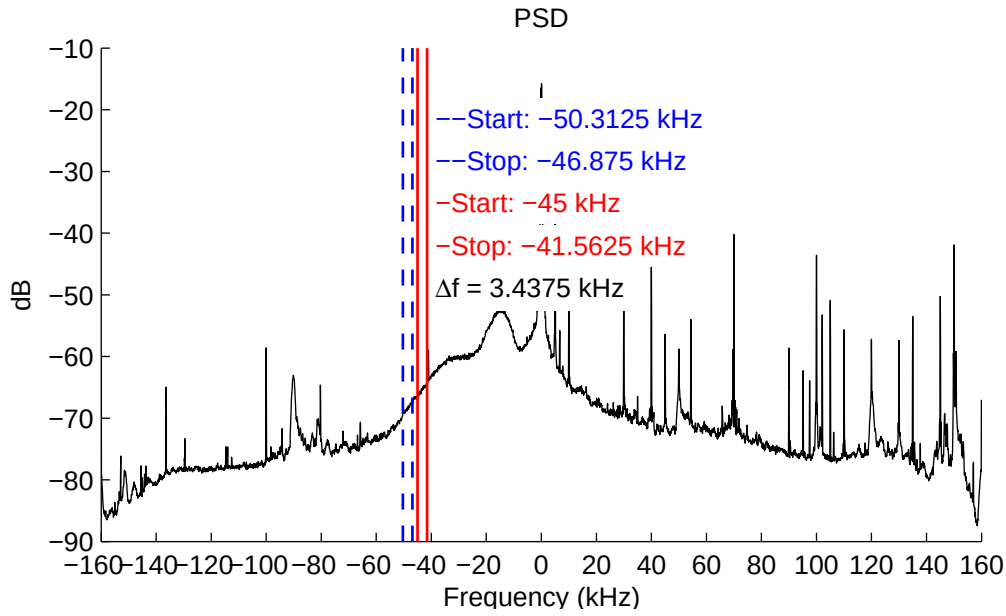

FIGURE 7.15: *Spectrum for trom99_520.*

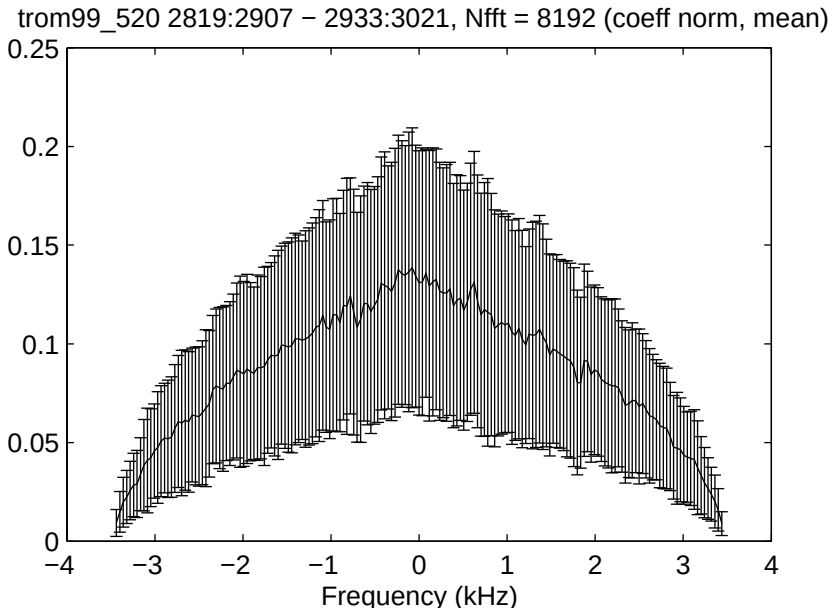

FIGURE 7.16: *Cross-correlation of the BC with 8192 data points per window (trom99_520). Mean of 200 windows. See figure 7.17 for spectrum.*

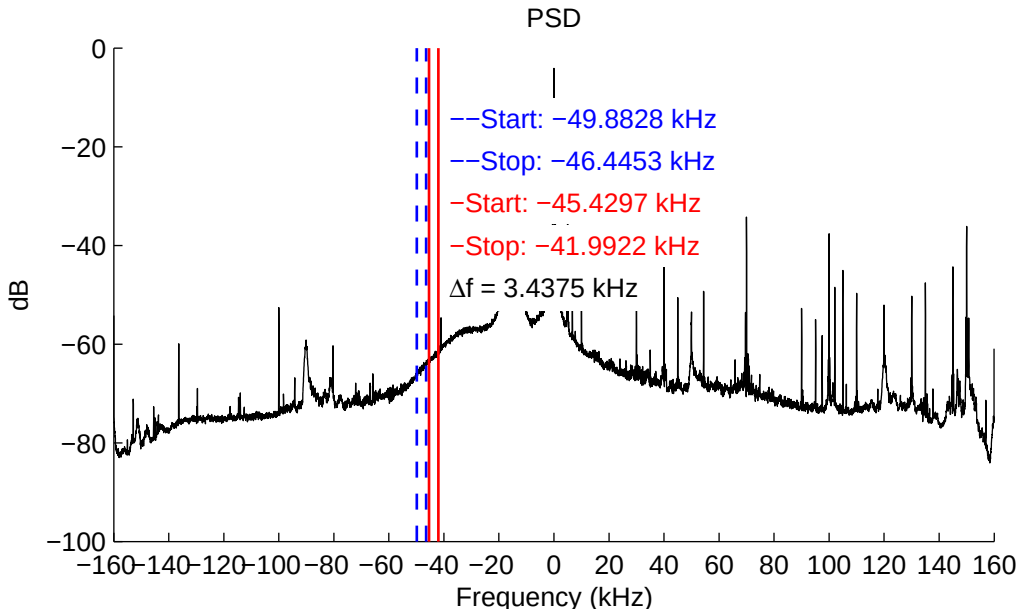

FIGURE 7.17: *Spectrum for trom99_520.*

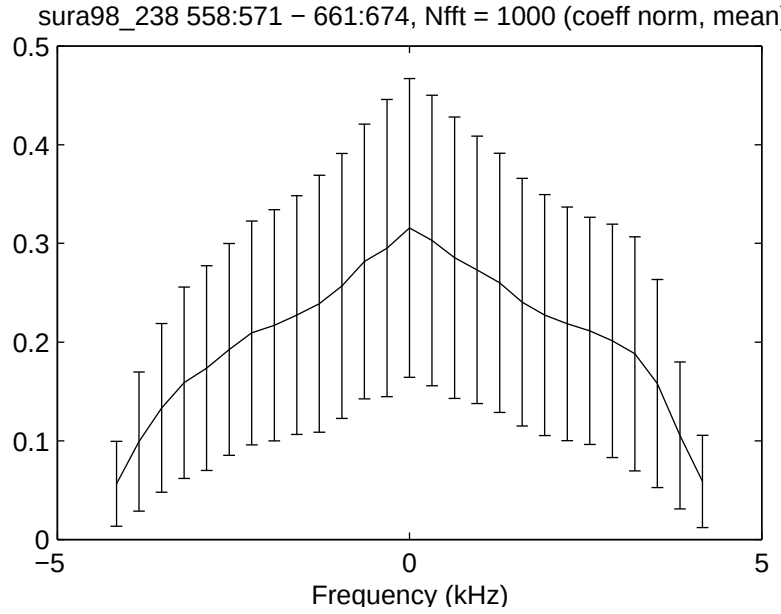

FIGURE 7.18: *The same cross-correlation as in figure 7.4, except that the mean consists of 1600 windows.*

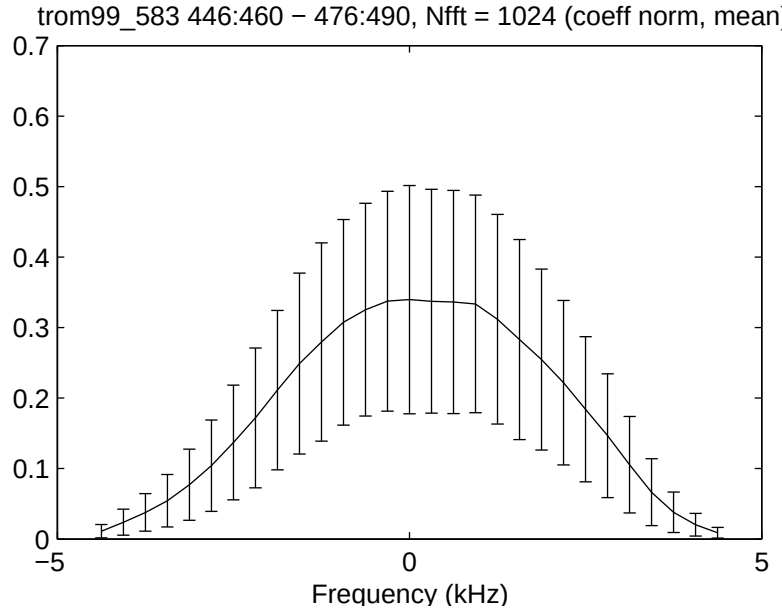

FIGURE 7.19: *Cross-correlation between the 2DM and DM (trom99_583). Mean of 1600 windows. See figure 7.20 for spectrum.*

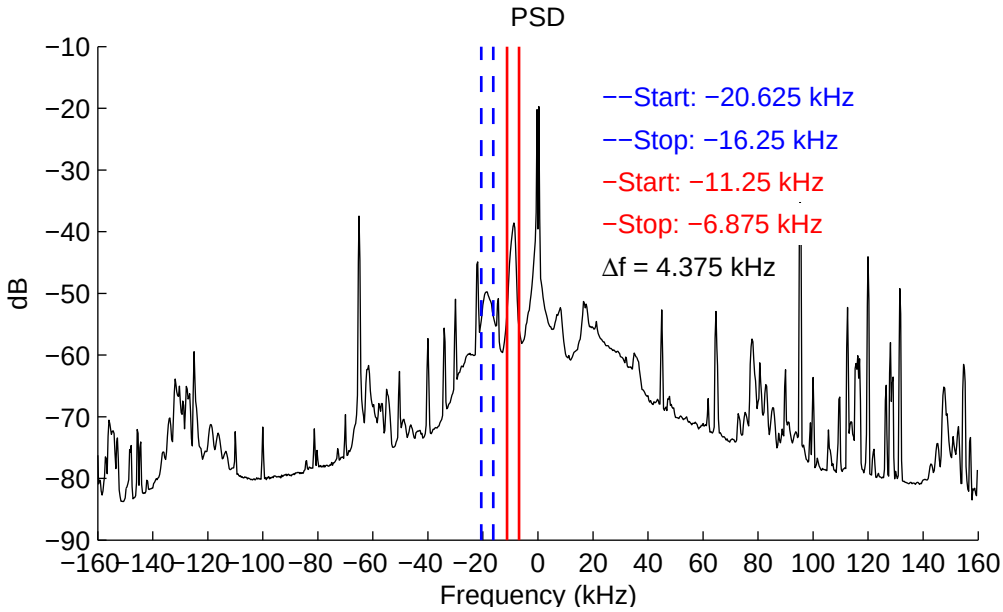

FIGURE 7.20: *Spectrum for trom99_583.*

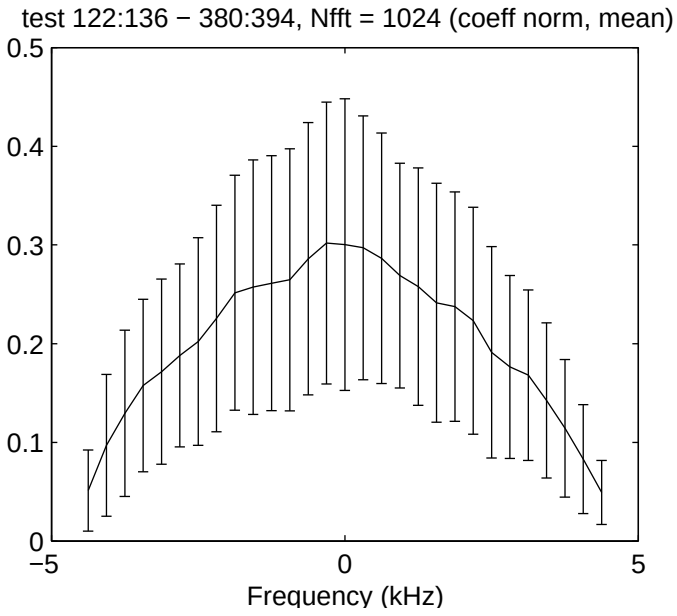

FIGURE 7.21: *Cross-correlation with standard deviation of two separate parts of a spectrum containing white noise. Mean of 200 windows.*

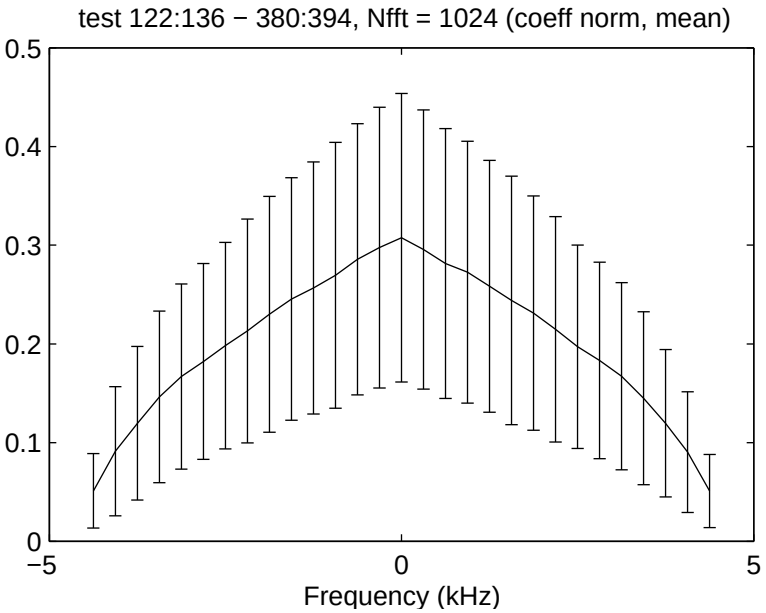

FIGURE 7.22: *Cross-correlation with standard deviation of two separate parts of a spectrum containing white noise. Mean of 1600 windows.*

7.2 Discussion

If the correlation between different frequencies is such that the resolution must be of the order of Hertz, each window must contain a high "density" of data points to show such a correlation. More data points per Hertz means longer windows in the time domain. But if the processes in the plasma have a certain coherence time, extending the windows and thus integrating over a greater period of time to get the Fourier spectrum, may destroy this coherence. Reducing the width of the windows narrows this risk, but also reduces the resolution.

To get a resolution of at least 100 Hz, the number of data points in each window must be over 3200. The lower limit of data points in each window was found to be about 1000 (depending on the length of the original time series; the total length of the time series must be evenly dividable with the length of the window), since this is the shortest window giving a reasonable amount of data points in the cross-correlation. Whether or not this length is sufficiently short to conserve the coherence is not known. The loss of correlation due to a too wide window is not justified by any other means than by reasoning: Over short periods, it should be possible to consider the process as stationary. But over greater periods of time, it may not be correct to consider it stationary.

The number of windows with length ~ 1000 required to see any patterns in the correlation was found to be $\gtrsim 40$. With a sampling frequency of 320 kHz and a window length of 1024 this corresponds to a time $T \gtrsim 130$ ms of usable data.

Chapter 8

Conclusion and Acknowledgements

8.1 Conclusion

Although the cross-correlation analysis method used in this work may not be the most refined (there are, for example, windowing methods that give much better resolution in frequency and time) it gives a small picture of what is going on. The complete lack of correlation in the SEE spectrum suggests that the transmitters in the ionosphere emit radiation incoherently. This can be caused by many processes, but one solution that is reasonable to assume is that the transmitters are moving in either direction in the ionosphere and thereby the resulting superposed electromagnetic radiation would appear noise-like.

This is however far from a closed case and much more thorough research in this area must be performed. New experimental campaigns should be performed with these kinds of analyses in mind (for example long pump duration should be used and strong spectral features to clearly separate them from noise are desired). Experiments to examine why the emissions are incoherent should also be conducted. Hopefully this work can inspire someone to look more into this.

8.2 Acknowledgements

I would like to thank all at the Swedish Institute of Space Physics, Uppsala (IRFU), and at the space physics part of the Department of Astronomy and Space Physics for making this a very pleasant half-year. Especially, I would like to thank my supervisor Ass. Prof. Thomas Leyser for giving me careful supervision and Jan-Ove Hall for spending time answering my questions and coming up with interesting views.

Appendix A

Program Code

A.1 Preparing the Data

The time series is split into several segments with the function `dela`.

```
1   function Y=dela(y, d, l)
2   % Function dela that takes a time series as input
3   % and divides it into d parts of length l, subtracts and tapers
4   % each segment with the Hamming window.
5   Y=reshape(y,l,d);
6   h=hamming(l);
7   for k=1:d
8       m=0;
9       % Mean is subtracted
10      m=mean(Y(:,k));
11      Y(:,k)=Y(:,k)-m;
12      % Multiplication with Hamming window
13      Y(:,k)=h.*Y(:,k);
14  end
```

Each column of the matrix output from the function `dela` is then Fourier transformed:

```
1   function X=transf(x)
2   % Fourier transforms a matrix with data
3   % records as columns.
4   [ro co]=size(x);
5   for k=1:co
6       X(:,k)=fftshift(fft(x(:,k)));
7   end
```

A.2 Bicoherence

MATLAB code for computing the bicoherence:

```
function b = bicohere(A)
% This function computes the bicoherence spectrum of a matrix.
% Input is a matrix with data records as columns.
[r,c]=size(A);
for l=1:0.5*r
    for k=1:l
        if (k+l)<=r*0.5
            % Reset all variables.
            B=0;
            Pk=0;
            Pl=0;
            Pkl=0;
            for i=1:c
                % Calculation of the bispectrum B
                B=B+(1/c)*A(k,i)*A(l,i)*conj(A((k+l),i));
                % Power spectrum for each component
                Pk=Pk+(1/c)*A(k,i)*conj(A(k,i));
                Pl=Pl+(1/c)*A(l,i)*conj(A(l,i));
                Pkl=Pkl+(1/c)*A(k+l,i)*conj(A(k+l,i));
            end
            % The bicoherence spectrum b
            b(k,l)=(abs(B)^2)/(Pk*Pl*Pkl);
        end
    end
end
```

A.3 Autocorrelation and Cross-correlation

Function for computing the autocorrelation:

```
function [C,f]=auto(C1, r)
% Computes the autocorrelation of a matrix with
% data records as columns.
[ro,co]=size(C1);
for k=1:co
    % Autocorrelation for each column
    C(:,k)=xcorr(C1(:,k),'coeff');
end
% Frequency f used to plot the autocorrelation function.
f=(320/(r))*(-ro+1:ro-1);
```

Function for computing the cross-correlation of two frequency windows:

```
1  function [C,f]=auto2(C1,C2,r)
2  % Computes the crosscorrelation of a matrix with
3  % data records as columns. C1 and C2 are the two
4  % frequency windows correlated.
5  [ro,co]=size(C1);
6  for k=1:co
7      % Crosscorrelation of each column
8      C(:,k)=xcorr(C1(:,k),C2(:,k),'coeff');
9  end
10 % Frequency f used to plot the cross-correlation
11 % function.
12 f=rot90(rot90((320/(r))*(-ro+1:ro-1)));
```

References

[1] T. B. Leyser. Stimulated electromagnetic emissions by high-frequency electromagnetic pumping of the ionospheric plasma. *Space Sci. Rev.*, 98:223–328, 2001.

[2] Bo Thidé. Electromagnetic radiation sensors and detectors. Unpublished material.

[3] John W. Tukey. An introduction to the calculations of numerical spectrum analysis. In Bernard Harris, editor, *Spectral Analysis of Time Series*. John Wiley & Sons, Inc., 1966.

[4] J. G. Luhmann. Ionospheres. In Margaret G-Kivelson and Christopher T. Russell, editors, *Introduction to Space Physics*, chapter 7. Cambridge University Press, 1995.

[5] T. D. Carozzi, B. Thidé, and T. B. Leyser. Full polarimetry measurements of stimulated electromagnetic emissions: First results. *J. Geophys. Res.*, 106(A10):21395–21407, 2001.

[6] D. R. Brillinger. *Time Series: Data Analysis and Theory*. International series in decision processes. Holt, Rinehart and Winston, Inc., 1975.

[7] M.B. Priestley. *Spectral analysis and time series*. Probability and mathematical statistics. Academic Press, 1989.

[8] Y. C. Kim and E. J. Powers. Digital Bispectral Analysis and Its Applications to Nonlinear Wave Interactions. *IEEE Trans. Plasma. Sci.*, PS-7:120–131, 1979.

[9] Y. C. Kim and E. J. Powers. Digital bispectral analysis of self-excited fluctuation spectra. *Phys. Fluids*, 21:1452–1453, 1978.

[10] W. B. Collis, P. R. White, and J. K. Hammond. Higher-order Spectra: The Bispectrum and Trispectrum. *Mechanical Systems and Signal Processing*, 12(3):375–394, 1998.

[11] D. B. Percival and A. T. Walden. *Spectral Analysis for Physical Applications*. Cambridge University Press, 1993.

[12] K. Hasselmann, W. Munk, and G. MacDonald. Bispectra of Ocean Waves. In M. Rosenblatt, editor, *Time Series Analysis*, The SIAM Series in Applied Mathematics, pages 125–139. John Wiley and Sons, Inc., 1963.

[13] John T. Rickard. On the Detection Theory of Autocoherence. *IEEE Transactions on information theory*, IT-31(1):80–90, 1985.

[14] Kasturi Rangan Krishnamachari, Robert E. Yantorno, Daniel S. Benincasa, and Stanley J. Wenndt. Spectral autocorrelation ratio as a usability measure of speech segments under co-channel conditions. IEEE International Symposium Intelligent Signal Processing and Communication Systems 2000, 2000.

[15] The MathWorks Inc. *Signal Processing Toolbox User's Guide*, 6 edition, December 2002.

[16] Fredric J. Harris. On the Use of Windows for Harmonic Analysis with the Discrete Fourier Transform. *Proceednings of the IEEE*, 66(1):51–83, 1978.

[17] Jens Trampe Broch. *Principles of Analog and Digital Frequency Analysis*. Tapir, 1981.